PRAMANA
— journal of
physics

© Indian Academy of Sciences

Vol. 66, No. 4
April 2006
pp. 765–780

Strangeness production in proton–proton and proton–nucleus collisions

RADHEY SHYAM
Saha Institute of Nuclear Physics, 1/AF, Bidhan Nagar, Kolkata 700 064, India
E-mail: radhey.shyam@saha.ac.in

Abstract. We discuss the investigation of the strange meson production in proton–proton (pp) and proton–nucleus (pA) reactions within an effective Lagrangian model. The kaon production proceeds mainly via excitations of $N^*(1650)$, $N^*(1710)$, and $N^*(1720)$ resonant intermediate nucleonic states, in the collision of two initial state nucleons. Therefore, the strangeness production is expected to provide information about the resonances lying at higher excitation energies. For beam energies very close to the kaon production threshold the hyperon–proton final state interaction effects are quite important. Thus, these studies provide a check on the models of hyperon–nucleon interactions. The in-medium production of kaons shows strong sensitivity to the self-energies of the intermediate mesons.

Keywords. Strangeness production; proton–proton collisions; proton–nucleus collisions; role of baryonic resonances.

PACS Nos 13.60.Le; 13.75.Cs; 11.80.-m; 12.40.Vv

1. Introduction

In the low-energy domain, quantum chromodynamics (QCD) is not amenable to the perturbation theory techniques. A compelling description of the QCD in this region could be achieved through Wilson's lattice guage theory [1]. These theories provide the most promising approach for the theoretical predictions of the properties of the hadronic ground states and also of their excited states. However, due to enormous computing power necessary for the numerical treatment, lattice QCD has only started to be able to describe baryon resonance masses and decay widths [2–4]. To simplify the problem a large number of quark models for hadrons (see, eg. [5]) have been developed which aim at predicting the properties of hadrons by reducing the complexity of the strongly self-interacting multi-quark-gluon system to an effective two- or three-quark system.

On the experimental side, the low-energy behavior of QCD is mostly addressed indirectly. The nucleon is excited with the help of a hadronic (nucleon or meson) or an electromagnetic (photon or electron) probe. However, due to extremely short life-time of the excited hadron states, measurement of only their decay products is possible. Consequently, experiments for investigating the inner structure of hadrons

have focused on meson production of the nucleon. Since, lattice QCD calculations are still far from being amiable to solutions for low and intermediate energy scattering reactions, it is necessary to use effective methods for the description of the dynamical structure of these processes. Such effective methods account for the inner structure of baryons by introducing explicitly baryon resonance states, whose properties are extracted by comparison with the experimental observables. The ultimate goal is to compare the values extracted in this way with those predicted by the lattice QCD calculations.

In recent years, there has been a considerable amount of interest in the study of the strangeness production reactions in proton–proton (pp) collisions. This is expected to provide information on the manifestation of QCD in the non-perturbative regime of energies larger than those of the low-energy pion physics where the low-energy theorem and partial conservation of axial current (PCAC) constraints provide a useful insight into the relevant physics [6]. The strangeness quantum number introduced by this reaction leads to new degrees of freedom into this domain which are expected to probe the admixture of $\bar{s}s$ quark pairs in the nucleon wave function [7] and also the hyperon–nucleon and hyperon–strange meson interactions [8,9].

The elementary nucleon–nucleon–strange meson production cross-sections are the most important ingredients in the transport model studies of the K^+-meson production in the nucleus–nucleus collisions, which provide information on not only the initial collision dynamics but also the nuclear equation of state at high density [10–17]. Furthermore, the enhancement in the strangeness production has been proposed as a signature for the formation of the quark-gluon plasma in high energy nucleus–nucleus collisions [18,19]. The understanding of the elementary reactions is a doorway to the investigation of the production of hypernuclei in reactions like $A(p, K^+)_\Lambda B$, where the hypernucleus ${}_\Lambda B$ has the same neutron and proton numbers as the target nucleus A, with one hyperon added.

The measurements performed in the late 1960s and 1970s provided the data on the total cross-sections for the associated hyperon (Y)–kaon production at beam momenta larger than 2.80 GeV/c (these cross-sections are listed in ref. [20]). With the advent of the high-duty proton-synchrotron (COSY) at the Forschungszentrum, Jülich, it has become possible to perform systematic studies of the associated strangeness production at beam momenta very close to the reaction threshold (see, e.g., ref. [21] for a comprehensive review). At the near-threshold beam energies, the final state interaction (FSI) effects among the outgoing particles are significant. Therefore, the new set of data are expected to probe the hyperon–nucleon and hyperon–strange meson interactions as well.

A very interesting result of the studies performed by the COSY-11 Collaboration is that the ratio (R) of the total cross-sections for the $pp \to p\Lambda K^+$ and $pp \to p\Sigma^0 K^+$ reactions (to be referred to as ΛK^+ and $\Sigma^0 K^+$ reactions, respectively) at the same excess energy (defined as $\epsilon = \sqrt{s} - m_p - m_Y - m_K$, with m_p, m_Y and m_K being the masses of proton, hyperon, and kaon respectively and s the invariant mass of the collision), is about 28^{+6}_{-9} for $\epsilon < 13$ MeV [22]. This result is very intriguing because at higher beam energies ($\epsilon \approx 1000$ MeV) this ratio is only around 2.5.

Several calculations have been reported [23–25] to explain this result. Assuming that the π- and K-exchange processes are the only mechanism leading to the strangeness production, Gasparian *et al* [23] show, within a (non-relativistic)

distorted wave Born approximation (DWBA) model, that while the ΛK^+ reaction is dominated by the K-exchange only, both K- and π-exchange processes play an important role in the case of $\Sigma^0 K^+$ reaction. Therefore, if the amplitudes corresponding to the two exchanges in the latter case interfere destructively, the production of Σ^0 is suppressed as compared to that of Λ. It should however, be noted that in ref. [24], K- and π-exchange amplitudes are reported to be of similar magnitudes for both ΛK^+ and $\Sigma^0 K^+$ reactions. In the calculations reported in ref. [25] also the relative sign of K- and π-exchange terms is chosen solely by the criteria of reproducing the experimental data, although in this work the theory has been applied to describe a wider range of data which includes the polarization transfer results of the DISTO experiment [26] and the missing mass distribution obtained in the inclusive K^+ production measurements performed at SATURNE [27] apart from the ratio R. Nevertheless, a conclusive evidence in support of the relative signs of π- and K-exchange amplitudes being opposite to each other is still lacking. Furthermore, other mechanisms like excitation, propagation, and decay of intermediate baryonic resonances which play (see, e.g., [28–30]) an important role in the strangeness production process, have not been considered by these authors.

We have investigated the ΛK^+ and $\Sigma^0 K^+$ reactions at near-threshold as well as higher beam energies in the framework of an effective Lagrangian approach (ELA) [28,29,31,32]. In this theory, the initial interaction between two incoming nucleons is modeled by an effective Lagrangian which is based on the exchange of the π-, ρ-, ω-, and σ-mesons. The coupling constants at the nucleon–nucleon–meson vertices are determined by directly fitting the T-matrices of the nucleon–nucleon (NN) scattering in the relevant energy region. The ELA uses the pseudovector (PV) coupling for the nucleon–nucleon–pion vertex which is consistent with the chiral symmetry requirement of the quantum chromodynamics [33]. In contrast to some earlier calculations [34], both ΛK^+ and $\Sigma^0 K^+$ reactions proceed via excitation of the $N^*(1650)$, $N^*(1710)$ and $N^*(1720)$ intermediate baryonic resonance states. The interference terms between the amplitudes of various resonances are retained. To describe the near-threshold data, the FSI effects in the final channel are included within the framework of the Watson–Migdal theory [32,35]. ELA has been used to describe rather successfully the $pp \to pp\pi^0$, $pp \to pn\pi^+$ [31,32], $pp \to pK^+Y$ [28,29] as well as $pp \to ppe^+e^-$ [36] reactions.

Within a similar approach we also investigate the (p, K^+) reaction. The initial interaction between the incoming proton and a bound nucleon of the target is described by the one-meson exchange processes. We use the same effective Lagrangians and vertex parameters to model these interactions. The initial state interaction between the two nucleons leads to the $N^*(1650)[\frac{1}{2}^-]$, $N^*(1710)[\frac{1}{2}^+]$, and $N^*(1720)[\frac{3}{2}^+]$ baryonic resonance intermediate states. The vertex parameters here too are the same as those used in the description of the elementary reaction.

2. Effective Lagrangian model

The idea of the effective Lagrangian models is to account for the symmetries of the QCD but including only effective degrees of freedom instead of quarks. These effective degrees of freedom are modeled by baryons and mesons known to exist as

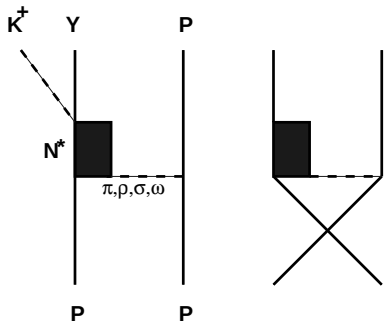

Figure 1. Feynman diagrams for K^+Y production in pp collisions. The diagram on the left shows the direct process while that on the right shows the exchange one.

(quasi-)bound quark states. The advantage is that in this way one gets a better insight into the underlying production mechanism which makes the interpretation of the results easier. However, due to a more complicated interaction structure, the meeting of the physical constraints like unitarity and analyticity becomes technically more involved. In fact, almost all the effective Lagrangian models are not analytic, many of them are not even unitary.

In our effective Lagrangian model, we consider the tree-level structure (figure 1) of the amplitudes for the associated K^+Y production in proton–proton collisions, which proceeds via the excitation of the $N^*(1650)[\frac{1}{2}^-]$, $N^*(1710)[\frac{1}{2}^+]$ and $N^*(1720)[\frac{3}{2}^+]$ intermediate resonances. The amplitudes are calculated by a summation of the Feynman diagrams generated by means of the effective Lagrangians at (a) the nucleon–nucleon–meson, (b) the resonance–nucleon–meson, and (c) the resonance–K^+–hyperon vertices. The assumption here is that the contributions of the higher-order diagrams are negligible or can be absorbed in the form factors of the first-order diagrams. The parameters for NN vertices are determined by fitting the NN elastic scattering T matrix with an effective NN interaction based on the π-, ρ-, ω- and σ-meson exchanges. The effective meson–NN Lagrangians are

$$\mathcal{L}_{NN\pi} = -\frac{g_{NN\pi}}{2m_N}\bar{\Psi}_N\gamma_5\gamma_\mu\boldsymbol{\tau}\cdot(\partial^\mu\boldsymbol{\Phi}_\pi)\Psi_N. \tag{1}$$

$$\mathcal{L}_{NN\rho} = -g_{NN\rho}\bar{\Psi}_N\left(\gamma_\mu + \frac{k_\rho}{2m_N}\sigma_{\mu\nu}\partial^\nu\right)\boldsymbol{\tau}\cdot\boldsymbol{\rho}^\mu\Psi_N. \tag{2}$$

$$\mathcal{L}_{NN\omega} = -g_{NN\omega}\bar{\Psi}_N\left(\gamma_\mu + \frac{k_\omega}{2m_N}\sigma_{\mu\nu}\partial^\nu\right)\omega^\mu\Psi_N. \tag{3}$$

$$\mathcal{L}_{NN\sigma} = g_{NN\sigma}\bar{\Psi}_N\sigma\Psi_N. \tag{4}$$

We have used the notations and conventions of Bjorken and Drell [37]. In eq. (1), m_N denotes the nucleon mass. Note that we have used a PV coupling for the $NN\pi$ vertex which is consistent with the chiral symmetry requirement. Since we use these Lagrangians to directly model the T-matrix, we have also included a nucleon–nucleon–axial-vector–isovector vertex, with the effective Lagrangian given by

$$\mathcal{L}_{NNA} = g_{NNA}\bar{\Psi}\gamma_5\gamma_\mu\boldsymbol{\tau}\Psi \cdot \mathbf{A}^\mu, \tag{5}$$

where $\mathbf{A}$ represents the axial-vector meson field. This term is introduced because in the limit of large axial meson mass (m_A) it cures the unphysical behavior in the angular distribution of NN scattering caused by the contact term in the one-pion exchange amplitude [38], if g_{NNA} is chosen to be

$$g_{NNA} = \frac{1}{\sqrt{3}} m_A \left(\frac{f_\pi}{m_\pi}\right), \tag{6}$$

with very large ($\gg m_N$) m_A. f_π in eq. (6) is related to $g_{NN\pi}$ as $f_\pi = (\frac{g_{NN\pi}}{2m_N})m_\pi$.

We introduce, at each interaction vertex, the form factor

$$F_i^{NN} = \left(\frac{\lambda_i^2 - m_i^2}{\lambda_i^2 - q_i^2}\right), \quad i = \pi, \rho, \sigma, \omega, \tag{7}$$

where q_i and m_i are the four momentum and mass of the ith exchanged meson, respectively. The form factors suppress the contributions of high momenta and the parameter λ_i, which governs the range of suppression, can be related to the hadron size. Since NN elastic scattering cross-sections decrease gradually with the beam energy (beyond a certain value), we take energy-dependent meson–nucleon coupling constants of the following form:

$$g(\sqrt{s}) = g_0 \exp(-\ell\sqrt{s}), \tag{8}$$

in order to reproduce these data in the entire range of beam energies. The parameters, g_0, λ and ℓ were determined by fitting to the elastic proton–proton and proton–neutron scattering data at beam energies in the range of 400 MeV to 4.0 GeV [31,38]. It may be noted that this procedure fixes also the signs of the effective Lagrangians (eqs. (1)–(5)). The values of various parameters are given in table 1 of ref. [28]. The same parameters for these vertices were also used in the calculations of the pion and the dilepton production in *pp* collisions. Thus we ensure that the NN elastic scattering channel remains the same in the description of various inelastic channels within this approach, as it should be.

Below 2 GeV center-of-mass (c.m.) energy, only three resonances, $N^*(1650)$, $N^*(1710)$ and $N^*(1720)$, have significant decay branching ratios into KY channels. Therefore, we have considered only these three resonances in our calculations. The $N^*(1700)$ resonance having very small (and uncertain) branching ratio for the decay to these channels, has been excluded. Since all the three resonances can couple to the meson–nucleon channels considered in the previous section, we require the effective Lagrangians for all the four resonance–nucleon–meson vertices corresponding to all the included resonances. Since the mass of the strange quark is much higher than that of the *u*- or *d*-quark, one does not expect the pion-like strict chiral constraints for the case of other pseudoscalar mesons like η and K (to be called ζ in the following). Thus, one has a choice of psuedoscalar (PS) or PV couplings for the $NN\zeta$ and $N^*_{1/2}N\zeta$ vertices (forms of the corresponding effective Lagrangians are given in ref. [28]). The same holds for the $N^*_{1/2}YK$ vertices also.

In principle, one can select a linear combination of both and fit the PS/PV ratio to the data. However, to minimize the number of parameters we choose either

PS or PV coupling at a time. In the results shown below, we have used PS couplings for both $N^*N\pi$ and $N^*\Lambda K^+$ vertices involving spin-1/2 resonances of even and odd parities. Calculations have also been performed with the corresponding PV couplings. The cross-sections calculated with this option for the $N^*_{1/2}YK$ vertex deviate very little from those obtained with the corresponding PS couplings. However, data show a clear preference for the PS coupling at the $N^*_{1/2}N\pi$ vertices.

The coupling constants for the vertices involving resonances are determined from the experimentally observed quantities such as branching ratios for their decays to corresponding channels. It may however, be noted that such a procedure cannot be used to determine the coupling constant for the $N^*(1650)\Sigma K$ vertices, as the on-shell decays of this resonance to ΣK channel are inhibited. Therefore, we have tried to determine this coupling constant by fitting the available data on the $\pi^+p \to \Sigma^+K^+$, $\pi^-p \to \Sigma^0K^0$ and $\pi^-p \to \Sigma^-K^+$ reactions in an effective Lagrangian coupled channels approach [39,40], where all the available data for the transitions from πN to five meson–baryon final states, πN, $\pi\pi N$, ηN, $K\Lambda$ and $K\Sigma$ are simultaneously analyzed for center-of-mass energies ranging from threshold to 2 GeV. In this analysis, all the baryonic resonances with spin $\leq \frac{3}{2}$ up to excitation energies of 2 GeV are included as intermediate states. Since the resonances considered in this study have no known branching ratios for the decay into the $N\omega$ channel, we determine the coupling constants for the $N^*N\omega$ vertices by the strict vector meson dominance (VMD) hypothesis [41], which is based essentially on the assumption that the coupling of photons on hadrons takes place through a vector meson.

It should be stressed that the branching ratios determine only the square of the corresponding coupling constants; thus their signs remain uncertain in this method. Predictions from independent calculations (e.g the quark model) can, however, be used to constrain these signs. The magnitude as well as signs of the coupling constants for the $N^*N\pi$, $N^*\Lambda K$, $N^*N\rho$ and $N^*N(\pi\pi)_{s\text{-wave}}$ vertices were determined by Feuster and Mosel [39] and Manley and Saleski [42] in their analysis of the pion–nucleon data involving the final states πN, $\pi\pi N$, ηN and $K\Lambda$. Predictions for some of these quantities are also given in the constituent quark model calculations of Capstick and Roberts [43]. Guided by the results of these studies, we have chosen the positive sign for the coupling constants for these vertices. Unfortunately, the quark model calculations for the $N^*N\omega$ vertices are still sparse and an unambiguous prediction for the signs of the corresponding coupling constants may not be possible at this stage [44]. Nevertheless, we have chosen a positive sign for the coupling constants for these vertices as well. Values of all the coupling constants are given in ref. [28].

After having established the effective Lagrangians, coupling constants and form of the propagators (which are given in ref. [28]), it is straightforward to write down the amplitudes for various diagrams associated with the $pp \to pYK$ reactions which can be calculated numerically by following e.g. the techniques discussed in [31]. The isospin part is treated separately. This gives rise to a constant factor for each graph, which is unity for the reaction under study. It should be noted that the signs of various amplitudes are fixed by those of the effective Lagrangian densities, coupling constants and propagators as described above. These signs are not allowed to change anywhere in the calculations.

In the present form of our effective Lagrangian theory, the energy dependence of the cross-section due to FSI is separated from that of the primary production amplitude and the total amplitude is written as

$$A_{fi} = M_{fi}(pp \to pYK^+) \cdot T_{ff}, \tag{9}$$

where $M_{fi}\,(pp \to pYK^+)$ is the primary associated YK production amplitude, while T_{ff} describes the re-scattering among the final particles which goes to unity in the limit of no FSI. The latter is taken to be the coherent sum of the two-body on-mass-shell elastic scattering amplitudes t_i (with i going from 1 to 3), of the interacting particle pairs $j - k$ in the final channel. This type of approach has been used earlier to describe the pion [32,45,46], η-meson [47–49], ΛK^+ [28] and ϕ-meson [50] production in pp collisions. An assumption inherent in eq. (9) is that the reaction takes place over a small region of space (which is fulfilled rather well in near-threshold reactions involving heavy mesons). Under this condition the amplitudes t_i can be expressed in terms of the inverse of the Jost function [32,35] which has been calculated using a Coulomb modified effective range expansion of the phase-shift [51]. The required effective range and scattering length parameters are given in refs [28,29].

3. Kaon production in proton–proton collisions

The total cross-sections for the ΛK^+ and $\Sigma^0 K^+$ reactions as a function of the excess energy are shown in figure 2. The calculations are the coherent sum of all resonance excitation and meson exchange processes as described earlier. In both cases a good agreement is obtained between theory and the data available from the COSY-11 Collaboration. Keeping in mind the fact that all parameters of the model, except for those of N^*Yp vertices and the FSI, were the same in the two calculations and that no parameter was freely varied, this agreement is quite satisfactory. It should be noted that we do not require to introduce arbitrary normalization constants to get the agreement between calculations and the data. We also show in this figure the results obtained without including the FSI effects (dashed line). It can be seen that the FSI effects are vital for a proper description of the experimental data in both the cases.

In figure 3, we have investigated the role of various meson exchange processes in describing the total cross-sections. The dashed, long-dashed, dashed–dotted, and solid curves with black squares represent the contributions of π-, ρ-, ω- and σ-meson exchanges, respectively. The contribution of the heavy axial meson exchange is not shown in this figure as it is negligibly small. The coherent sum of all the meson exchange processes is shown by the solid line. It is clear that the pion exchange graphs dominate the production process for both the reactions in the entire range of beam energies. Contributions of ρ- and ω-meson exchanges are almost insignificant. On the other hand, the σ-meson exchange, which models the correlated s-wave two-pion exchange process and provides about 2/3 of this exchange in the low-energy NN interaction, plays a relatively more important role. This observation has also been made in the case of the $NN \to NN\pi$ reaction [52–54,31].

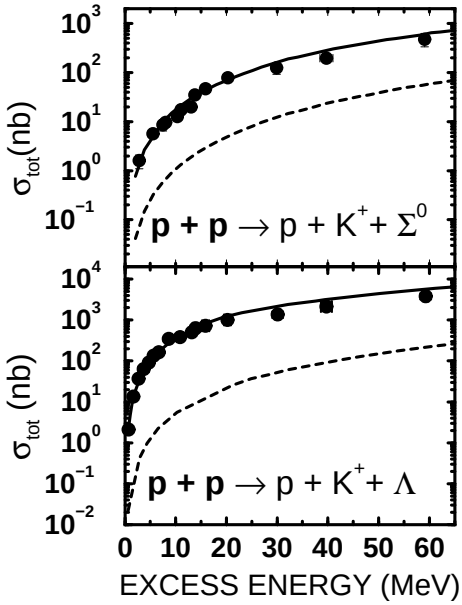

Figure 2. Comparison of the calculated and the experimental total cross-sections for the $pp \to p\Lambda K^+$ and $pp \to p\Sigma^0 K^+$ reactions as a function of the excess energy. Results obtained with no FSI effects are shown by dashed lines. The experimental data are from ref. [22].

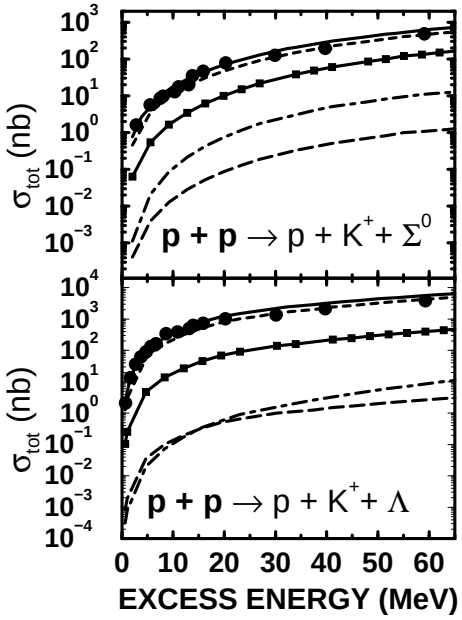

Figure 3. Contributions of various meson exchange processes to the total cross-section for the $pp \to pK^+\Lambda$ and $pp \to pK^+\Sigma^0$ reactions. The dashed, long-dashed, dashed–dotted and solid curves with black squares represent the contributions of π-, ρ-, ω- and σ-meson exchanges, respectively. Their coherent sums are shown by the solid lines. The solid circles represent the experimental data taken from ref. [22].

The individual contributions of various nucleon resonances to the total cross-sections of the two reactions are shown in figure 4. We note that in both the cases, the cross-section is dominated by the $N^*(1650)$ resonance excitation for $\epsilon < 30$ MeV. Since $N^*(1650)$ is the lowest energy baryonic resonance having branching ratios for the decay to YK^+ channels, its dominance in these reactions at beam

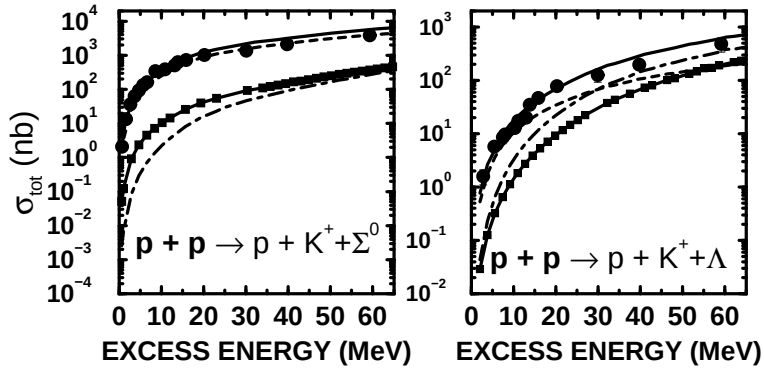

Figure 4. Contributions of $N^*(1650)$ (dashed line), $N^*(1710)$ (solid line with black squares) and $N^*(1720)$ (dashed–dotted line) baryonic resonances to the total cross-section for the two reactions studied in figure 2. Their coherent sum is shown by the solid line. The solid circles show the experimental data taken from ref. [22].

energies very close to the kaon production threshold is to be expected. In the near-threshold region the relative dominance of various resonances is determined by the dynamics of the reaction where the difference of about 60 MeV in excitation energies of $N^*(1650)$ and $N^*(1710)$ resonances plays a crucial role. However, for ϵ values between 30 and 60 MeV, while the $pp \to pK^+\Lambda$ reaction continues to be dominated by the $N^*(1650)$ excitation, the $pp \to pK^+\Sigma^0$ reaction also gets significant contributions from the $N^*(1710)$ and $N^*(1720)$ resonances. This difference in the role of the three resonances in the two cases can be understood in the following way. For a resonance to contribute significantly, we should have $m_Y + m_K + \epsilon \geq m_{N^*} + \Gamma_{N^*}/2$, where m_{N^*} and Γ_{N^*} are the mass and width of the resonance, respectively. Therefore, in the region of excess energies $\geq Q[= (m_{N^*} + \Gamma_{N^*}/2) - (m_Y + m_K)]$, the particular resonance N^* should contribute significantly. The values of Q for the $pp \to pK^+\Lambda$ reaction are 115 MeV, 150 MeV and 185 MeV, for the $N^*(1650)$, $N^*(1710)$ and $N^*(1720)$ resonances, respectively. On the other hand, for the $pp \to pK^+\Sigma^0$ case, they are 36 MeV, 72 MeV and 105 MeV, respectively for these three resonances. Therefore, contributions of the $N^*(1710)$ and $N^*(1720)$ resonance excitations are negligibly small for the $K^+\Lambda$ production in the entire energy range of the COSY-11 data (i.e., for $\epsilon \leq 60$ MeV) while they are significant for the $K^+\Sigma^0$ case for $\epsilon > 30$ MeV. It would be helpful to have data on the invariant mass spectrum at these excess energies in order to confirm these theoretical observations.

In figure 5, we compare our calculations with the data for the ratio R as a function of ϵ. We have shown here the results for excess energies up to 60 MeV, where the COSY-11 data are available. It is clear that our calculations can describe well the trend of the fall-off of R as a function of the excess energy. It should be noted that FSI effects account for about 60–80% of the observed ratio for $\epsilon < 30$ MeV and about 50% beyond this energy. Therefore, not all of the observed value of R at these beam energies can be accounted for by the FSI effects, which is in agreement with the observation made in [23]. It should again be emphasized that without considering the contributions of the $N^*(1650)$ resonance for the $\Sigma^0 K^+$ reactions,

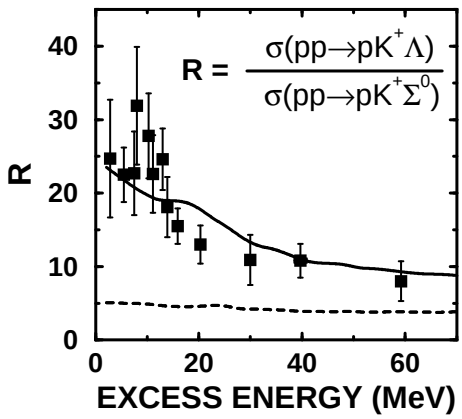

Figure 5. Ratio of the total cross-sections for $pp \to p\Lambda K^+$ and $pp \to p\Sigma^0 K^+$ reaction as a function of the excess energy. The solid and dashed lines show the results of our calculations with and without FSI effects, respectively. The data are from ref. [22].

the calculated ratio would be at least an order of magnitude larger. Therefore, these data are indeed sensitive to the details of the reaction mechanism. At higher beam energies ($\epsilon > 300$ MeV), values of R obtained with and without FSI effects are almost identical. In this region the reaction mechanism is different; here all the three resonances contribute in one way or the other, their interference terms are significant [28], and FSI related effects are unimportant.

4. Kaon production in proton–nucleus collisions

The study of meson production in proton–nucleus collisions is an interesting tool to investigate the influence of nuclear medium on the properties of hadrons and their production processes. Since the mass of kaon is larger than that of the pion, medium effects play a vital role in its production in pA collisions.

The kaon production reactions of the type $p + A(N, Z) \to {}_\Lambda B(N, Z) + K^+$ (where N and Z are the neutron and proton numbers, respectively, in the target nucleus A), leads to the production of the Λ-hypernucleus ${}_\Lambda B(N, Z)$. The study of this reaction, therefore, is likely to lead to an understanding of the hypernuclear spectroscopy. At the same time, since this reaction involves a large momentum transfer to the nucleus, it provides an appropriate tool to learn about the behaviour of the nuclear many-body wave function at higher momenta which is not very well-known. We present here some results of our investigation for this reaction which will be referred to as $A(p, K^+)_\Lambda B$ reaction.

The model used to describe the (p, K^+) reaction is similar to the effective Lagrangian approach described above (see, figures 6a and 6b). The initial interaction between the incoming proton and a bound nucleon of the target is described by the one-meson exchange mechanism. We use the same effective Lagrangians and vertex parameters to model these interactions. The initial state interaction between the

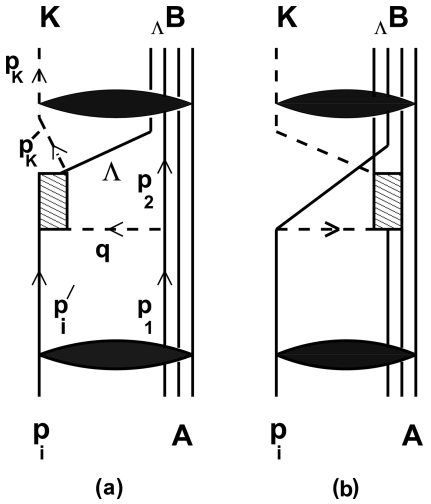

Figure 6. Graphical representation of the $A(p, K^+)_\Lambda B$ reaction models. The elliptic shaded area represent the optical model interactions in the incoming and outgoing channels.

two nucleons leads to the $N^*(1650)[\frac{1}{2}^-]$, $N^*(1710)[\frac{1}{2}^+]$ and $N^*(1720)[\frac{3}{2}^+]$ baryonic resonance intermediate states. The vertex parameters here too are the same as those used in the description of the elementary reactions. It may be noted that in this model there are altogether three active bound state baryon wave functions taking part in the reaction process allowing the large momentum transfer to be shared among the three baryons. Consequently, the sensitivity of the model is shifted from high momentum parts of the bound state wave functions (not very well-known) to those at relatively lower momenta where they are rather well-known from the $(e, e'p)$ and (γ, p) experiments (see, e.g., [55]) and are relatively larger. This type of two-nucleon model has recently been applied to the study of the $A(p, K^+)_\Lambda B$ reaction in refs [56,57] where to reduce the computational complications plane waves have been used to describe the relative motions of incoming proton and outgoing kaon.

In performing calculations for the cross-sections of the $A(p, K^+)_\Lambda B$ reactions, one requires spinors for the final bound hypernuclear state (corresponding to momentum p_Λ) and for two intermediate nucleonic states (corresponding to momenta p_1 and p_2). These are determined by assuming them to be pure single-particle or single-hole states with the core remaining inert. The quantum numbers of the two intermediate states are taken to be the same. The spinors in the momentum space are obtained by Fourier transformation of the corresponding coordinate space spinors which are obtained by solving the Dirac equation with potential fields consisting of an attractive scalar part and a vector part with the Woods–Saxon geometry. With a fixed set of geometry parameters, the depths of the potentials are searched in order to reproduce the binding energies of the particular state [57].

To have an idea of the relative strengths of the upper and lower components of the Dirac spinors as a function of the transferred momentum, we show, e.g., in figure 7 the $0p_{3/2}$ Λ hyperon spinors in momentum space for the ${}^{41}_{\Lambda}$Ca hypernucleus.

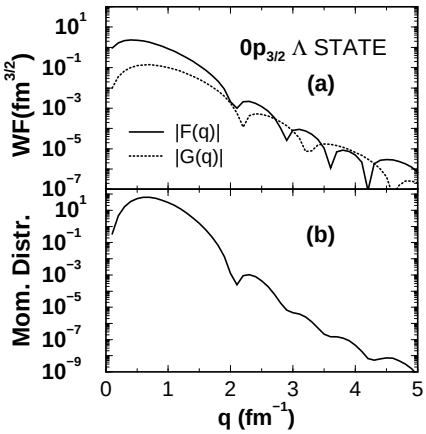

Figure 7. (**a**) Momentum space spinors (WF) for $0p_{3/2}$ Λ orbit in ${}^{41}_{\Lambda}$Ca hypernucleus. $|F(q)|$ and $|G(q)|$ are the upper and lower components of the spinor, respectively. (**b**) Momentum distribution (Mom. Distr.) for the same state calculated with wave functions shown in (a).

We note that only for momenta <1.5 fm^{-1}, is the lower component of the spinor substantially smaller than the upper component. In the region of momentum transfer pertinent to exclusive kaon production in proton–nucleus collisions, the magnitudes of the upper and lower components are of the same order of magnitude. This clearly demonstrates that a fully relativistic approach is essential for an accurate description of this reaction.

The self-energies of the exchange mesons are other input quantities required in the calculations of the $A(p, K^+)_\Lambda B$ reaction. They take into account the medium effects on the intermediate meson propagation. The ρ and ω self-energies have been calculated by following the procedure described in ref. [58]. The pion self-energy is more crucial as one-pion exchange diagrams dominate the (p, K^+) cross-sections. This is obtained by calculating the contribution of particle–hole (ph) and delta–hole (Δh) excitations produced by the propagating pion [59]. This has been renormalized by including the short-range repulsion effects by introducing the constant Landau–Migdal parameter g' which is taken to be the same for ph–ph and Δh–ph and Δh–Δh correlations which is a common choice. The parameter g', acting in the spin–isospin channel, is supposed to mock up the complicated density-dependent effective interaction between particles and holes in the nuclear medium. Most estimates give a value of g' between 0.5–0.7. The sensitivity of the pion self-energy $[\Pi(q)]$ to the g' parameter is studied in ref. [56].

In figure 8, we show the kaon angular distributions corresponding to various final hypernuclear states excited in the reaction ^{40}Ca$(p, K^+){}^{41}_{\Lambda}$Ca. We have taken $g' = 0.5$ throughout in this figure. It may be noted that in all the cases the diagram 6a makes a dominant contribution to the cross-sections. Clearly, the cross-sections are quite selective about the excited hypernuclear state, being maximum for the state of largest orbital angular momentum. This is due to the large momentum transfer involved in this reaction. We see in this figure that in each case the angular

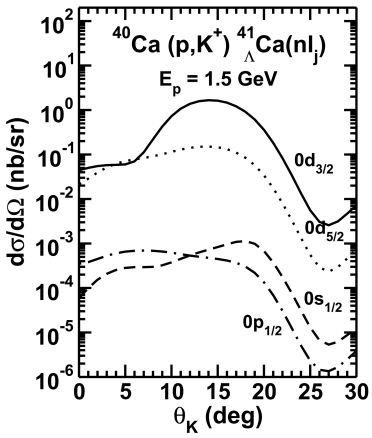

Figure 8. Differential cross-section for the ^{40}Ca$(p, K^+)^{41}_{\Lambda}$Ca reaction for the incident proton energy of 1.5 GeV for various bound states of final hypernucleus as indicated in the figure. The Λ separation energies for $0d_{3/2}$, $0d_{5/2}$, $0p_{1/2}$ and $0s_{1/2}$ states were taken to be 0.7529, 1.5435, 9.1400 and 17.8802 MeV, respectively. The quantum number and the binding energy of the two intermediate nucleon states were $0d_{3/2}$ and 8.3282 MeV, respectively.

distribution has a maximum at angles larger than the zero degree and not at the zero degree as seen in previous non-relativistic calculations of this reaction. This is the consequence of using Dirac spinors for the bound states. There are several maxima in the upper and lower components of the momentum space-bound spinors in the region of large momentum transfers. Therefore, in the kaon angular distribution the first maximum may shift to larger angles.

In figure 9, we show the dependence of our calculated cross-sections on pion self-energy. It is interesting to note that the self-energy has a rather large effect. We also see a surprisingly large effect on the short-range correlation (expressed schematically by the Landau–Migdal parameter g') on the cross-sections.

The absolute magnitudes of the cross-sections near the peak is around 1–2 nb/sr, although the distortion effects could reduce these values as is shown in [57]. This order-of-magnitude estimates should be useful in planning future experiments for this reaction. As found in ref. [56], contributions from the $N^*(1710)$ resonance dominate the total cross-section in each case. Also the interference terms of the amplitudes corresponding to various resonances are not negligible. It should be emphasized that we have no freedom in choosing the relative signs of the interference terms.

5. Summary and conclusions

In summary, our effective Lagrangian model can describe well the recent data on $pp \to p\Lambda K^+$ and $pp \to p\Sigma^0 K^+$ reactions. An important result is that the $N^*(1650)$ resonant state contributes predominantly to both these reactions at near-threshold

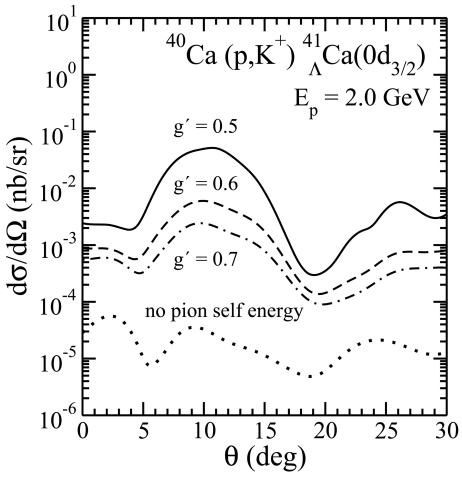

Figure 9. Differential cross-section for the $^{40}\mathrm{Ca}(p, K^+)^{41}_{\Lambda}\mathrm{Ca}(0d_{3/2})$ reaction for the incident proton energy of 2.0 GeV. The dotted line shows the results obtained without including the pion self-energy in the denominator of the pion propagator while solid line, dashed line and dashed–dotted lines represent the same calculated with pion self-energy renormalized with Landau–Migdal parameters of 0.5, 0.6 and 0.7, respectively.

beam energies. Therefore, these reactions in this energy regime, provide an ideal means of investigating the properties of this S_{11} baryonic resonance. To the extent that the final state interaction effects in the exit channel can be accounted for by the Watson–Migdal theory, our model is able to explain the experimentally observed large ratio of the total cross-sections of the two reactions in the near-threshold region.

We also investigated the $A(p, K^+)_{\Lambda}B$ reaction within a similar approach. We find that the nuclear medium corrections to the intermediate pion propagator introduce large effects on the kaon differential cross-sections. There is also the sensitivity of the cross-sections to the short-range correlation parameter g' in the pion self-energy. Thus, (p, K^+) reactions may provide an interesting alternative tool to investigate the medium corrections on the pion propagation in nuclei. Moreover, the study of the (p, K^+) reaction is attractive as it provides a way to study the spectroscopy of the Λ hypernuclear states. This reaction should be measurable at the COSY facility in Forschungszentrum Jülich. The characteristics of these cross-sections predicted by us should be helpful in planning such experiments.

Acknowledgements

The author wishes to acknowledge useful discussions with Bo Höistad, Göran Fäldt, Anders Ingemarsson, Horst Lenske, Ulrich Mosel, Walter Oelert and Gregor Penner.

References

[1] K G Wilson, *Phys. Rev.* **D10**, 2445 (1974)
[2] J M Zanotti, S Bilson-Thompson, F D R Bonnet, P D Coddington, D B Leinweber, A G Williams, J B Zhang, W Lelnitchouk and F X Lee, *Phys. Rev.* **D65**, 074507 (2002)
[3] S Sakai, T Blum and S Ohta, *Phys. Rev.* **D65**, 074503 (2002)
[4] D B Leinweber, A W Thomas, A G Williams, R D Young, J M Zanotti and J B Zhang, *Nucl. Phys.* **A737**, 177 (2004)
[5] L Theussl and R F Wagenbrunn, *Phys. Rev.* **C64**, 068201 (2001)
L Theussl, R F Wagenbrunn, B Desplanques and W Plessas, *Euro. Phys. J.* **A12**, 91 (2001); *Nucl. Phys.* **A689**, 394 (2001)
[6] T E O Ericson and W Weise, *Pions and nuclei* (Clarendon, Oxford, 1988)
[7] M Alberg, *Prog. Part. Nucl. Phys.* **36**, 217 (1996)
[8] A Deloff, *Nucl. Phys.* **A505**, 583 (1989)
[9] R A Adelseck and B Saghai, *Phys. Rev.* **C42**, 108 (1990)
[10] U Mosel, *Ann. Rev. Nucl. Part. Sci.* **41**, 29 (1991) and references therein
[11] G E Brown, C M Ko, Z G Wu and L H Xia, *Phys. Rev.* **C43**, 1881 (1991)
[12] T Maruyama, W Cassing, U Mosel, S Teis and K Weber, *Nucl. Phys.* **A573**, 653 (1994)
[13] D Miskowiec *et al*, *Phys. Rev. Lett.* **72**, 3650 (1994)
[14] C Hartnack, J Jaenicke, L Sehn, H Ströcker and J Aichelin, *Nucl. Phys.* **A580**, 643 (1994)
[15] X S Fang, C M Ko, G Q Li and Y M Zheng, *Nucl. Phys.* **A575**, 766 (1994)
[16] G Q Li and C M Ko, *Phys. Lett.* **B349**, 405 (1995)
[17] G Q Li, C M Ko and W S Chung, *Phys. Rev.* **C57**, 434 (1998)
[18] J Rafelski and B Müller, *Phys. Rev. Lett.* **48**, 1066 (1982)
[19] H W Barz, B L Friman, J Knoll and H Schulz, *Nucl. Phys.* **A485**, 685 (1988)
[20] Landolt-Börnstein, *Numerical data and functional relationships in science and technology*, *New Series* edited by H Schopper, I/12 (Springer, Berlin, 1988)
[21] P Moskal, M Wolke, A Khoukaz and W Oelert, *Prog. Part. Nucl. Phys.* **49**, 1 (2002)
[22] S Sewerin *et al*, *Phys. Rev. Lett.* **83**, 682 (1999)
P Kowina *et al*, *Euro. Phys. J.* **A22**, 293 (2004)
[23] A M Gasparian, J Haidenbauer, C Hanhart, L Kondratyuk and J Speth, *Phys. Lett.* **B480**, 273 (2000)
[24] A Sibirtsev, K Tsushima, W Cassing and A W Thomas, LANL preprint, nucl-th/0004022
[25] J M Laget, *Nucl. Phys.* **A691**, 11c (2001); *Phys. Lett.* **B359**, 24 (1991)
[26] F Balestra *et al*, *Phys. Rev. Lett.* **83**, 1534 (1999)
[27] R Siebert *et al*, *Nucl. Phys.* **A567**, 819 (1994)
[28] R Shyam, *Phys. Rev.* **C60**, 055213 (1999)
[29] R Shyam, G Penner and U Mosel, *Phys. Rev.* **C63**, 022202(R) (2001)
[30] G Fäldt and C Wilkin, *Z. Phys.* **A357**, 241 (1997)
[31] A Engel, R Shyam, U Mosel and A K Dutt-Majumdaer, *Nucl. Phys.* **A603**, 387 (1996)
[32] R Shyam and U Mosel, *Phys. Lett.* **B425**, 1 (1998)
[33] S Weinberg, *Phys. Rev.* **166**, 1568 (1996)
[34] A Sibirtsev, K Tsushima and A W Thomas, *Phys. Lett.* **B421**, 59 (1998)
A Sibirtsev, K Tsushima, W Cassing and A W Thomas, *Nucl. Phys.* **A646**, 427 (1999)

[35] M L Goldberger and K M Watson, *Collision theory* (Wiley, New York, 1969) pp. 549
[36] R Shyam and U Mosel, *Phys. Rev.* **C67**, 065202 (2003)
[37] J D Bjorken and S D Drell, *Relativistic quantum mechanics* (McGraw-Hill, New York, 1964)
[38] M Schäfer, H C Dönges, A Engel and U Mosel, *Nucl. Phys.* **A575**, 429 (1994)
[39] T Feuster and U Mosel, *Phys. Rev.* **C58**, 457 (1998); **C59**, 460 (1999)
[40] G Penner and U Mosel, *Phys. Rev.* **C66**, 055211 (2002); **66**, 055212 (2002)
[41] J J Sakurai, *Currents and mesons* (Univ. of Chicago Press, Chicago, 1969); *Ann. Phys.* **11**, 1 (1960)
[42] D M Manley and E M Saleski, *Phys. Rev.* **D45**, 4002 (1992)
[43] S Capstick and W Roberts, *Phys. Rev.* **D49**, 4570 (1994)
[44] Fl Stancu and P Stassart, *Phys. Rev.* **D46**, 2140 (1993)
[45] J Dubach, W M Kloet and R R Silbar, *Phys. Rev.* **C33**, 373 (1986)
[46] V Bernard, N Kaiser and Ulf-G Meissner, *Euro. Phys. J.* **A4**, 259 (1999)
[47] A Moalem, E Gedalin, L Razdolskaja and Z Shorer, *Nucl. Phys.* **A600**, 445 (1996)
[48] B L Druzhinin, A E Kudryavtsev and V E Tarasev, *Z. Phys.* **A359**, 205 (1997)
[49] A Deloff, *Phys. Rev.* **C69**, 035206 (2004)
[50] A I Titov, B Kämpfer and B L Reznik, *Euro. Phys. J.* **A7**, 543 (2000)
[51] H P Noyes, *Ann. Rev. Nucl. Sci.* **22**, 465 (1972)
[52] V Dmitriev, O Sushkov and C Gaarde, *Nucl. Phys.* **A459**, 503 (1986)
[53] T S H Lee and D O Riska, *Phys. Rev. Lett.* **70**, 1137 (1993)
[54] C J Horowitz, H O Meyer and D K Griger, *Phys. Rev.* **C49**, 1337 (1994)
[55] S Frullani and J Mougey, *Adv. Nucl. Phys.* **14**, 1 (1984)
[56] R Shyam, H Lenske and U Mosel, *Phys. Rev.* **C69**, 065205 (2004)
[57] R Shyam, H Lenske and U Mosel, LANL preprint, nucl-th/0505043
[58] P Mühlich, T Falter and U Mosel, *Euro. Phys. J.* **A20**, 499 (2004)
[59] V F Dmitriev and Toru Suzuki, *Nucl. Phys.* **A438**, 697 (1985)